Upconverted luminescence from nonequilibrium vibronic states of Cr ions in forsterite

S. G. Demos and R. R. Alfano

Institute for Ultrafast Spectroscopy and Lasers, Department of Physics,
The City College and Graduate School of the City University of New York, New York, New York 10031

Nonequilibrium excited vibronic states of photoexcited Cr^{4+} ions in a forsterite crystal were studied using picosecond laser excitation and ultrasensitive photon counting detection. The excitation involves the absorption of two photons per photoexcited ion by means of excited-state absorption. Discrete peaks are observed in the hot upconverted luminescence spectrum and are attributed to the population of nonequilibrium vibronic levels during the deexcitation of the ions by phonon emission. This work reveals some of the phonon modes participating in the nonradiative relaxation of the photoexcited ions. The shape of the luminescence spectral envelope suggests a bottleneck in the nonradiative decay at about 2.1 eV from coupling between the ^1E and $^3T_1$ states.

I. INTRODUCTION

Photoexcitation of an impurity ion in a crystal is followed by nonradiative and radiative relaxation processes. In transition metal-doped materials or F centers, within picoseconds after photoexcitation the electronic system reaches a metastable storage level (SL) and the rapid phonon emission concludes.[1-5] The lifetime of the SL is of the order of microseconds or longer.[6] The excess energy coming from the difference in energy between the excitation level and the SL is released in the lattice in the form of phonons. During this process nonequilibrium vibronic levels are populated with energy separation equal to the energy of the emitted phonons. From these short-lived vibronic levels there is a probability for radiative relaxation to the ground state[7,8] resulting in a weak luminescence called hot luminescence (HL). Hot luminescence has been observed in various dielectric crystals.[9,10] The observed weak signal of HL occurs at frequencies lower than the excitation frequency and typically overlaps with the Stokes Raman-scattering components. The overlapping of the HL with the peaks of the Raman-scattering emission prevents the observation of the fine structure in the HL spectrum. The HL fine structure is a signature of the initial steps of the cascade process directly showing which phonon modes are involved in the vibrational relaxation. In semiconductors, the presence of an acceptor level discriminates the HL signal from the Raman signal.[11,12] The HL emission is due to the recombination of electrons with neutral acceptors and consequently this emission occurs at energies lower than the Raman scattering. The recombination of unrelaxed carriers with neutral acceptors has been observed in GaAs showing a series of peaks from the energy loss of hot electrons by LO phonon emission.[11-15] The first peak in the HL spectra of GaAs arises from the transition from the excitation level (no phonon emitted) to the acceptor level. In dielectric crystals, phonon peaks involving the lowest states of the molecular anharmonic oscillator[16] have been observed in F centers with substitutional molecular defects.

In transition metal-doped materials, ordinary luminescence (OL) occurs from the long-lived storage levels or nearby thermally populated electronic states. In some crystal systems, conversion of low-wave into short-wave radiation is possible by multiphoton absorption. This mechanism is called upconversion. Green upconverted OL has been observed in MgF_2:Ni^{2+} under photoexcitation by 752.5 nm (Ref. 17) radiation. This emission arises from a higher metastable level populated by excited-state absorption (ESA). Upconversion processes have been extensively studied in rare-earth ion-doped crystals.[18] In 1987 the first laser action upon upconversion was reported[19] in $YAlO_3$:Er^{3+} crystal, demonstrating that ESA can be a very efficient way to populate higher-lying electronic states.

In this paper, we report the observation of hot luminescence following ESA in Cr^{4+}-doped forsterite, a tunable solid-state laser crystal. The excitation level is higher than the photon energy by an amount of energy equal to the energy of the storage level. Therefore, hot luminescence from the excitation level and the vibronic levels underneath that are populated during the vibrational relaxation is blue shifted with respect to the laser wavelength. The observed upconverted HL spectrum is isolated from any of the other photoemission processes. Following photoexcitation, the excited ions relax by emitting phonons. As a result a cascade of vibronic levels is populated spaced by one phonon energy apart. The use of a two-step photoexcitation technique allows the observation of fine vibrational structure in the upconverted hot luminescence emission associated with the nonequilibrium vibronic levels. The observed phonon peaks reveal information on the nonequilibrium phonon modes involved in the vibrational relaxation decay of the photoexcited ions. Our work provides information on which modes participate in the initial steps of the nonradiative decay of an excited impurity ion; this has not been documented before experimentally. In addition, we show in the present paper that the spectral profile reveals an electronic bottleneck occurring at ≈ 2.1 eV where the upper ^1E and $^3T_1$ electronic states overlap.

II. EXPERIMENTAL TECHNIQUE

The schematic diagram depicting the upconverted two-step hot luminescence process is shown in Fig. 1. Absorption of the laser light by the ions quickly produces a highly populated storage level. In the case of excited-state absorption the center absorbs a photon, while it is temporally relaxing at the storage level (SL) and reaches an excitation level (EL) at energy

$$E_{EL} = E_{SL} + h\nu_{laser} \ . \tag{1}$$

This process requires two steps and in the case of low in energy ultrashort pulses, the photons originate from different pulses. The time separation between two pulses should be smaller than the lifetime of the storage level because a populated SL should be available when the second pulse arrives. The upconverted HL spectrum involves downward radiative transitions from the manifold of nonequilibrium electronic-vibrational states populated during the vibrational relaxation of the ions.

The experimental arrangement consists of a cw mode-locked Nd:YAG laser operating at 82 MHz, a synchronously pumped dye laser, a triplemate spectrograph, and an ultrasensitive photon counting image acquisition system (PIAS) (Hamamatsu model C1815). The 1064 nm laser beam from the Nd:YAG laser and the tunable output of the Rh6G dye laser were the excitation sources. The laser power was ≈ 400 mW, while the pulsewidth was ≈ 5 psec. The sample is a forsterite crystal (Cr^{4+}:Mg_2SiO_4) of $10 \times 10 \times 2$ mm^3 in dimension containing 0.02 at. % of Cr^{4+}. In Cr^{4+}-doped Forsterite[20–23] only the $^3T_2 \rightarrow {}^3A_2$ infrared transition has been reported. Using two-step photoexcitation the higher-lying vibrational levels of the $^3T_1$ electronic state were populated. The experimental setup is shown in Fig. 2. The laser beam is focused into the sample using a short focal length lens, while the fluorescence light is collected and focused into the spectrograph by an 85 mm camera lens. Two scattering geometries were utilized. In Fig. 2(a) the backscattering (BS) configuration is shown. A 3-mm-
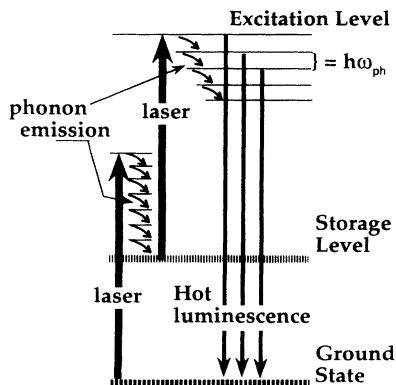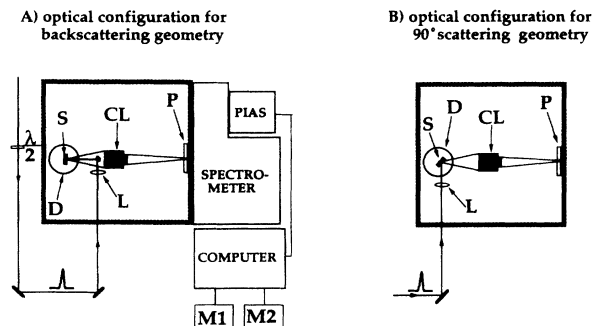
FIG. 2. Experimental setup of the optical configuration for (a) backscattering geometry and (b) for 90° scattering geometry (S: sample, CL: camera lens, L: lens, P: polarizer, D: optical cryostat, M1 and M2: computer monitors 1 and 2).

diam mirror in front of the camera lens directs the focused by an 8 cm focal length lens laser beam into the sample. Figure 2(b) displays the second scattering geometry (PS), where the direction of the laser beam is perpendicular to the direction of light collection, while the sample is placed at 45° with respect to excitation beam. The photon counting image acquisition system was used to detect the upconverted HL signal. The PIAS detector is attached to a SPEX triplemate spectrograph. An optical cryostat was used for the low-temperature experiments. The experiments were performed at room- and liquid-nitrogen temperatures. ESA was possible, since the time interval between consecutive pulses is 12 ns, while the lifetime of the SL is 3–25 μs depending on the temperature.[21]

III. EXPERIMENTAL RESULTS

Figure 3 shows HL spectra for different excitation wavelengths. Ions in the SL (1.137 eV, $^3T_2$ state) absorb a photon to reach a higher-lying vibrational level (EL) of the $^3T_1$ state within the ESA process. Using 617 nm (2.01 eV) laser pulse for excitation, the energy of the excitation level is $E_{EL} = 3.147$ eV ($= 1.137 + 2.01$). Figure 3(a) shows the emission spectrum measured at $T = 80$ K in BS geometry. The polarization of the excitation beam (P_e) and the polarizer in the collection path (P_s) were parallel to the c axis of the crystal. This luminescence signal shows a series of peaks with the highest energy peak positioned at exactly the excitation level $E_{EL} = 3.15$ eV. Figure 3(b) displays spectra taken using pump wavelengths at 626 nm to reach $E_{EL} = 3.118$ eV and 614 nm to reach $E_{EL} = 3.157$ eV. Notice, the spectral profiles are similar, while the highest energy peak shifts proportionally to the laser frequency shift [$E_{EL} = E_{SL} + h\nu_{laser}$]. In these cases, the first peak appears at the excitation level energy. The spacing between the remaining peaks is 513 ± 12 and 325 ± 12 cm^{-1}. This behavior indicates that the signal indeed arises from hot luminescence, since in these cases it is expected that the spectral profiles are independent of small pumping wavelength shifts.[24]

Pumping with 1064 nm (1.165 eV) laser light, the first HL peak following ESA appears at 2.302 eV

FIG. 1. Schematic diagram of the upconverted hot luminescence process.
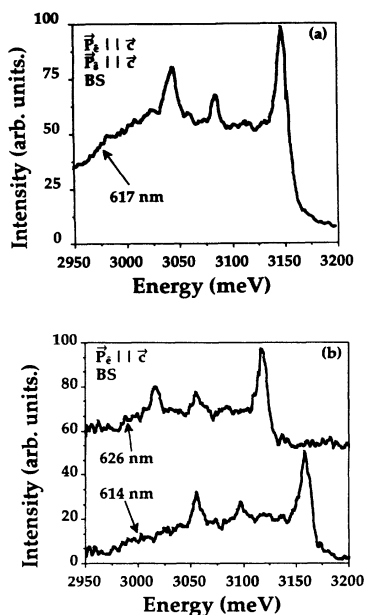
FIG. 3. Hot luminescence spectra following excited-state absorption under (a) 617-nm excitation and (b) 614-nm (upper profile) and 626-nm excitation (lower profile) at liquid-nitrogen temperature.

(1.137+1.165). Figure 4 displays the HL spectra under 1064 nm excitation for the BS geometry and for $P_e \| b$ axis at liquid-nitrogen temperature. Figures 4(a) and 4(b) show HL spectra taken with $P_s \| b$ axis and $P_s \| c$ axis of the crystal, respectively. Using excitation polarization $P_e \| c$ axis, the spectra are practically identical to the spectra taken with $P_e \| b$ axis showing that the HL spectral profiles are independent of the polarization of the excitation laser beam. However, the HL intensity is reduced by a factor of ≈ 4. Figures 5(a) and 5(b) show HL spectra for the PS geometry. Although the relative intensity of the peaks change, their energies remain the same. The intensities of the peaks in all spectra strongly depend on the luminescence polarization. The location of the peaks in energy is the same in all spectra under 1064 nm excitation. The spacing between the peaks are different occurring at ≈ 323 and ≈ 218 cm^{-1}. The room-temperature HL spectra displayed in Figs. 6(a) and 6(b) show no well-defined peak structure but the overall spectral envelope has a similar shape to the low-temperature spectra. All spectra shown in Figs. 4, 5, and 6 exhibit a characteristic increase of intensity at ≈ 2.1 eV. The HL tail at energies lower than 1.8 eV is observable but not shown in our figures, since it does not carry any new information. The intensity of the lower energy emission tail is approximately equal to the HL intensity exhibited at 1.85 eV and shown in our figures. The integrated intensity at 2.1 eV is about 10 times larger than at 1.85 eV.

The peak structure in the upconverted HL spectrum is due to emission from the higher-lying vibronic levels of the $^3T_1$ state. These vibronic levels are populated during the transfer of energy from the ion to the lattice environment by phonon emission. We can now study which are the phonons involved in this process by measuring the en-
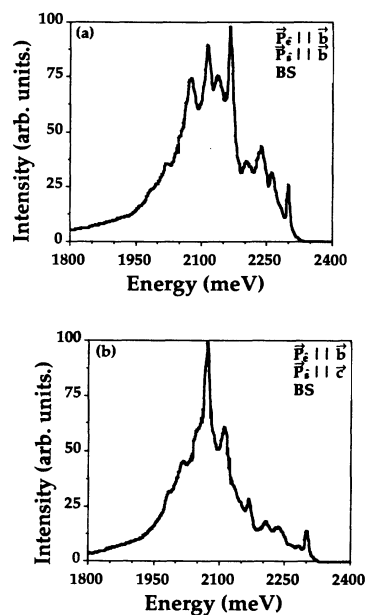
FIG. 4. Upconverted hot luminescence under 1064 nm excitation. The laser polarization (P_e) is parallel to the b axis and the emission polarization (P_s) is (a) $P_s \| b$ and (b) $P_s \| c$ axis of the crystal at backscattering geometry (BS). The sample was at liquid-nitrogen temperature.

ergy separation of the peaks observed in the upconverted HL spectrum. The measured differences in energy between successive peaks are shown in Table I for 617 and 1064 nm excitation wavelengths. Under 617-nm laser excitation, two peaks appear following the highest energy
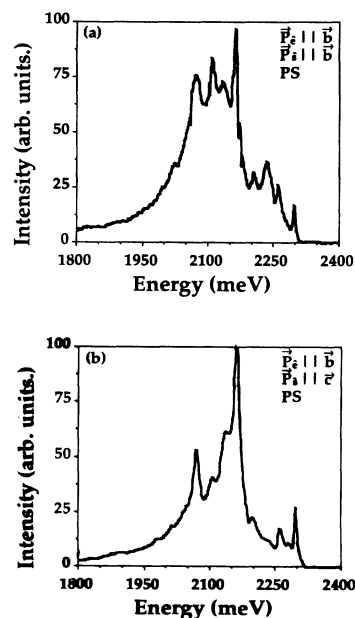
FIG. 5. Upconverted hot luminescence under 1064-nm excitation. $P_e \| b$ axis and (a) $P_s \| b$ or (b) $P_s \| c$ axis of the crystal. The experimental conditions are 90° scattering geometry (PS) with the sample at liquid-nitrogen temperature.

zero-phonon peak. The energy separation is 513 ± 12 and 325 ± 12 cm^{-1}, indicating the phonon modes participating in the relaxation process of the excited state located at 3.15 eV. Excitation of the sample with 1064 nm allows the observation of the phonon modes participating in the vibronic relaxation of the part of the excited state located at 2.3 eV above the ground state. The energy separation of these peaks are given in Table I indicate that there are two modes participating centered at 323 and 218 cm^{-1}.

IV. THEORETICAL APPROACH

A. Hot luminescence

To explain the observed salient spectral feature described above, the following model is presented. The probability for radiative transition from the nth vibrational level of the excited state (T) to the mth vibrational level of the ground state (g) is given by the well-known expression[6]

$$W_{Tn-gm} \sim \frac{2\pi}{h^2}|\langle \Psi_g(r_i,Q)|\boldsymbol{\mu}\cdot\hat{\boldsymbol{\varepsilon}}|\Psi_T(r_i,Q)\rangle\rangle|\mathbf{E}|\langle\chi_g(m)|\chi_T(n)\rangle\rangle|^2 , \tag{2}$$

where the integration is over the electron and vibrational coordinates, μ is the appropriate electronic dipole operator, and $\hat{\varepsilon}$ the unit polarization vector of the electric field intensity ($\mathbf{E}=\hat{\varepsilon}\cdot E$). The relative values of W_{Tn-gm} depend on the squares of the vibrational overlap integrals. The vibrational wave functions $\chi_T(n)$ and $\chi_g(m)$ are each a similar set of harmonic oscillator functions but are defined with respect to different zeros of the configurational coordinate Q.

The shape and intensity of the emission spectrum arising from radiative transitions from the nth vibrational level of the excited state to any of the vibrational levels of the ground state is given by

$$I_{T,n}(E)=I_0R_{T,n}\sum_m P_{Tn-gm}|\langle\chi_g(m)|\chi_T(n)\rangle\rangle|^2\delta(E_{T,n}-E_{g,m}-E) , \tag{3}$$

where P_{Tn-gm} is the purely electronic transition probability between the excited state and the ground state and $R_{T,n}$ indicates the average excited-state population in the nth vibronic level of the excited state.[6] When the point of maximum amplitude of $\chi_T(n)$ is aligned with the middle of the ground-state parabola Q_0 [maximum amplitude of $\chi_g(0)$], the transition $\chi_T(n)\rightarrow\chi_g(0)$ will be dominant leading to a strong zero-phonon peak followed by weak sidebands.[6] The reason is that the vibrational integral

$|\langle\chi_g(0)|\chi_T(n)\rangle\rangle|$ is larger than other combinations of $\chi_T(n)$ with $\chi_g(m\neq0)$. The emission of a phonon will lead to a vibrational wavefunction $\chi_T(n-1)$, which will have its maximum amplitude at a point shifted with respect to Q_0. The photoemission spectrum from this vibronic level will be characterized by a strong peak arising from the $\chi_T(n-1)\rightarrow\chi_g(0)$ transition but the relative intensity of the sideband will increase. The difference in energy between the zero-phonon peaks $[\chi_T(n)\rightarrow\chi_g(0)$ and $\chi_T(n-1)\rightarrow\chi_g(0)]$ will be equal to the energy of the emitted phonon. After the emission of a sufficient num-

FIG. 6. HL under 1064 nm excitation. Experimental conditions are $P_e\|b$ axis, (a) $P_s\|b$ and (b) $P_s\|c$ axis of the crystal. The scattering geometry is PS and the sample is at room temperature.

TABLE I. Energy separation between successive peaks under 617 and 1064 nm laser excitation.

excitation wavelength	phonon peak	Energy difference between successive phonon peaks (cm^{-1})
617 nm	1	513 ± 12 cm^{-1}
	2	325 ± 12 cm^{-1}
1064 nm	1	323 ± 20 cm^{-1}
	2	218 ± 20 cm^{-1}
	3	226 ± 20 cm^{-1}
	4	323 ± 20 cm^{-1}
	5	218 ± 20 cm^{-1}
	6	210 ± 20 cm^{-1}
	7	323 ± 20 cm^{-1}

ber of phonons (i), the point of maximum amplitude of $\chi_T(n-i)$ will be very different from Q_0 producing a spectrum having a broad band with no peaks. The shape of the overall hot luminescence spectrum will be given by the sum of the different components $I_{T,n}(E)$ representing the superposition of the spectral profiles due to each vibronic level. The zero-phonon peaks $[\chi_T(n-i)\rightarrow\chi_g(0)]$ should be positioned on top of a broadband background coming from the superposition of the vibrational sidebands. The intensity of the peaks should diminish after the emission of a number of phonons and the rest of the HL signal should be observable throughout the excited-state band until the beginning of the ordinary luminescence. These features should dominate in the low-temperature spectrum where SL is well defined.

Crossings between electronic levels in the configurational diagram will deform the potential energy curve causing lower vibronic relaxation rates of the ionic system. Lifetimes on the order of picoseconds are expected from these "trapping" states depending on the coupling strengths. Since the excited ions relax passing through the same nonequilibrium excited-state vibronic levels, the average occupation number of each level (parameter $R_{T,n}$ in Eq. 3) is proportional to its lifetime. The HL emission from the vibronic levels within this electronic bottleneck will be more intense. This is because the excited ions are occupying these levels for longer period of time resulting to an increased overall probability for radiative transition to the ground state. The ratio of the total integrated intensities of the HL emission from the different vibronic levels should be approximately equal to the ratio of their lifetimes.[24]

B. Upconverted hot luminescence in forsterite

In order to use the above model to explain the observed upconverted HL spectra in forsterite, we take into account that at low temperature only the zero vibrational levels $[\chi_g(0)]$ of the ground state ($^3A_2$) and $[\chi_{SL}(0)]$ of the SL ($^3T_2$) are populated. The position of the maximum amplitudes of the vibrational wavefunctions $\chi_{SL}(0)$ and $\chi_g(0)$ are slightly shifted with respect to each other due to the small Huang-Rhys factor $S\leq0.4$ in forsterite.[25] A Cr^{4+} ion in the $\chi_{SL}(0)$ state absorbs a photon to reach a higher excited state having vibrational wave function $\chi_T(s)$ at the point Q_0 of the excited-state configurational coordinates parabola. This process is depicted in Fig. 7. In the photoemission spectrum from $\chi_T(s)$, the transition leading to zero vibrational level $\chi_g(0)[\chi_T(s)\rightarrow\chi_g(0)]$ of the ground state will be dominant. This transition appears as the highest-energy peak. As the excited Cr^{4+} ions relax down the ladder of the electronic manifold emitting phonons, the position of maximum amplitude of $\chi_T(n)$ shifts and the intensity of the zero-phonon transition decreases, while the intensity of the vibrational sideband increases. Further emission of phonons leads to a continuous broadband spectrum associated with the radiation transitions from $\chi_T(n)$. The overall upconverted HL spectra profile is a superposition of all these components and appears as a sharp line at ex-
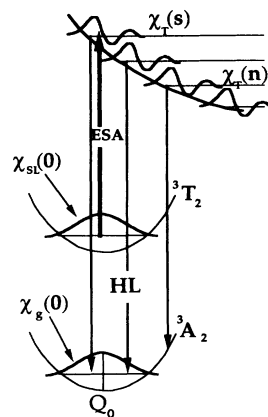
FIG. 7. Schematic diagram showing the relation between the vibrational wavefunctions $\chi_i(m)$ and upconverted HL in forsterite.

actly the excitation level followed by other peaks on top of a background and at decreasing energy ending in a broadband emission with no structure. At high temperatures, the thermal population of many vibrational levels of the metastable level will produce a broad storage level. The ESA from the broad SL produces also broad vibronic levels that overlap resulting in the loss of the fine structure in the HL spectrum. The overall profile remains the same, reflecting the excited-state band characteristics. HL spectra taken under 614, 617, and 626 nm excitation shown in Fig. 3 have all of the above characteristics. On the other hand, the spectra shown in Figs. 4, 5, and 6 taken under 1064 nm excitation exhibit the additional feature of the enhancement of the HL emission at 2.1 eV. This enhancement can be explained in terms of a slowing down of the nonradiative relaxation in this region due to crossing between the ^1E and $^3T_1$ states, which will be discussed in the next section.

V. DISCUSSION

The HL spectra from the ≈3.15 eV levels reached after pumping with ≈617 nm and ESA show the emission of two phonons, one 513 ± 12 cm^{-1} followed by a 325 ± 12 cm^{-1} phonon. Pumping with 1064 nm leads to HL from levels below 2.3 eV. The separation between the peaks in the latter spectra is ≈218 and ≈323 cm^{-1} indicating the phonons emitted during the vibronic relaxation below 2.3 eV. This shows the different nonradiative relaxation dynamics associated with various parts of the excited state. The 513 cm^{-1} mode is an internal mode of the tetrahedral (SiO_4), while the 218- and 323-cm^{-1} modes can be assigned either to translational modes of the Mg ion or external modes of the ($-SiO_4$).[26] Although more than one phonon modes are involved in the vibrational relaxation, the peaks in the upconverted HL spectra are well defined. This suggests that the sequence that the phonons are emitted is predetermined by the ion-lattice interaction dynamics. At this time, we do not have any explanation for these rather unexpected result.

The experiments also demonstrate the dependence of the upconverted HL on the emission polarization (Figs. 4 and 5). This dependence is expected, since it is a common characteristic in the OL emission spectra in transition metal-doped materials and it has been reported in forsterite.[21] Furthermore, it has been shown that the upconverted HL spectrum does not depend on the excitation polarization. The spectral profiles remain the same for the different laser polarizations. This indicates that the ions immediately after excitation "forget" how they were excited and that the "pathway" down the electronic manifold is unique.

ESA under 1064-nm excitation will excite Cr ions to a level 2.302 eV above the ground state. This level can also be reached by direct absorption of 539 nm photons where forsterite absorbs strongly. Therefore, a strong two-step absorption is expected under 1064-nm excitation, resulting in a significant HL signal. On the other hand, two-step excitation with 620 nm photons is equivalent to absorption of one 395-nm photon for which the sample exhibits very little absorption. This explains why the HL signal under 620-nm excitation is ≈ 100 times weaker than spectra taken under 1064-nm excitation.

From the Tanabe-Sugano energy-level diagram of forsterite the upper ^1E and $^3T_1$ electronic states are predicted to be at about 2.01 eV. A small peak on the absorption spectra is located at 1.97 eV and has been assigned to the ^1E state.[23,27] The absorption bands of the ^1E and the $^3T_1$ electronic states overlap in this region. The crossing of the ^1E with the $^3T_1$ state as shown on Fig. 8 produces an electronic bottleneck trap that delays the nonradiative decay of the excited electron-lattice system. This bottleneck is apparent in all HL spectra obtained under 1064-nm excitation (Figs. 4, 5, and 6) as an enhancement of the signal arising from levels with energy 2.1 ± 0.2 eV. The relative intensity of the average HL signal at 2.1 eV over the signal at 1.85 eV is over 10-fold, which means that the ratio of the lifetimes of these levels is of the same order. These results indicate that a significant slowing down of the nonradiative relaxation process is taking place at about 2.1 eV due to the crossing of these two bands. Typical lifetimes of the vibrational levels are of the order of 100 fs[4]. Therefore, from the intensity ratio, the lifetime of the states inside the bottleneck should be of the order of 1 ps. The upconverted HL spectra under 1064-nm excitation shows that the electronic bottleneck extends from ≈ 2.30 to 1.95 eV containing approximately 12 vibronic levels. Assuming that the lifetime of each level is about 1 ps, the expected overall time that the excited ions need to cross the electronic bottleneck states is on the order of 10 ps. This was confirmed by streak camera measurement of this emission that was performed giving an overall decay time of approximately 10 ps for the HL originated in the electronic bottleneck.
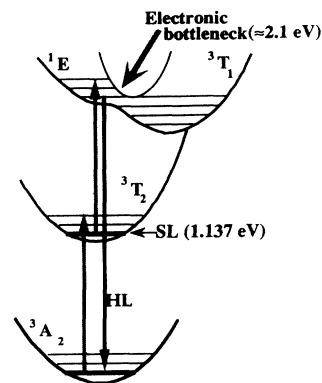
FIG. 8. Energy diagram of Cr^{4+} in forsterite. The ^1E electronic state is crossing the $^3T_1$ state causing an electronic bottleneck.

The upconverted two-step HL technique allows the study of the relaxation dynamics of the upper excited states. Due to the two photon absorption process, the upconverted HL is blue shifted with respect to the excitation source preventing any overlapping with the Raman signal or luminescence from other impurity centers which are red-shifted processes. This selective isolation of the HL signal allows the observation of the peak structure in the HL profile and subsequently the determination of which phonon modes are involved in the nonradiative decay. In addition, information concerning the potential surfaces and electronic bottlenecks can be extracted. From our work, several questions need to be addressed by theoreticians concerning the modes involved in the vibronic relaxation of the upper electronic states and the underlying physics. The electronic bottleneck at 2.1 eV clearly observed in the upconverted HL spectra, is very difficult to detect using direct pumping. Only a strong emission on top of the anti-Stokes room-temperature Raman spectrum that appears when the laser photon energy is less than 2.1 eV is an indication of the presence of this electronic bottleneck. This is due to anti-Stokes HL emission following the population of vibronic states within the bottleneck via absorption of light by thermally excited ions in the ground state.

The technique presented here can be used in a variety of systems in order to study the characteristics of the upper excited states and the nonradiative processes.

ACKNOWLEDGMENTS

[1]L. A. Riseberg and H. W. Moos, Phys. Rev. **174**, 429 (1968).

[2]N. Robertson and L. Friedman, Philos. Mag. **33**, 753 (1976).

[3]C. W. Struck and W. H. Fonger, J. Lumin. **10**, 1 (1975).

[4]J. M. Wiesenfeld, Linn F. Mollenauer, and Erich Ippen, Phys. Rev. Lett. **47**, 1668 (1981).

[5]A. M. Stoneham, Philos. Mag. **36**, 983 (1977).

[6]B. Henderson and G. F. Imbusch, *Optical Spectroscopy of Inorganic Solids* (Wiley, New York, 1989), Chaps. 5 and 9.

[7]K. Peuker and E. D. Trifonov, Phys. Status Solidi 30, 479 (1968).

[8]V. Hizhnyakov and I. Tehver, Phys. Status Solidi 39, 67 (1970).

[9]Yuzo Mori, Ryo Hattori, and Hiroshi Ohkura, J. Phys. Soc. Jpn. 51, 2713 (1982).

[10]Y. Kondo, T. Noto, S. Sato, and M. Hirai, J. Lumin. 38, 164 (1987).

[11]B. P. Zacharchenya, V. D. Dymnikov, I. Ya. Karlik, D. N. Mirlin, L. P. Nikitin, V. I. Perel, and I. I. Reshina, J. Phys. Soc. Jpn. 49, Suppl. A 573, (1980).

[12]D. N. Mirlin, I. Ya. Karlik, L. P. Nikitin, I. I. Reshina, and V. F. Sapega, Solid State Comm. 37, 757 (1981).

[13]B. P. Zacharchenya, J. Lumin. 24/25, 669 (1981).

[14]G. Fasol and H. P. Hughes, Phys. Rev. B 33, 2953 (1986).

[15]C. L. Petersen and S. A. Lyon, Phys. Rev. Lett. 65, 760 (1990).

[16]P. Saari and K. Rebane, Solid State Comm. 7, 887 (1969); Yihong Yang, Wolf von der Osten, and Fritz Luty, Phys. Rev. B 32, 2724 (1985).

[17]R. Moncorge, F. Auzel, and J. M. Breteau, Philos. Mag. B 51, 489 (1985); R. Moncorge and T. Benyattou, Phys. Rev. B 37, 9186 (1988).

[18]E. W. J. L. Oomen, J. Lumin. 50, 317 (1992).

[19]A. Silversmith, W. Lenth, and R. M. Macfarlane, Appl. Phys. Lett. 54, 2301 (1989).

[20]V. Petricevic, S. K. Gayen, R. R. Alfano, K. Yamagishi, H. Anzai, and Y. Yamaguchi, Appl. Phys. Lett. 52, 1040 (1988); Appl. Phys. Lett. 53, 2590 (1988).

[21]H. R. Verdun, L. M. Thomas, D. M. Andrauskas, T. McCollum, and A. Pinto, Appl. Phys. Lett. 53, 2593 (1988); *OSA Proceedings of the Advanced Solid-State Lasers,* edited by M. L. Shand and H. P. Jenssen (Optical Society of America, Washington, D.C., 1989), Vol. 15, p. 85.

[22]R. Moncorge, G. Cormier, D. J. Simkin and J. A. Capobianco, J. Quantum Electr. 27, 114 (1991).

[23]Weiyi Jia, Huimin Liu, S. Jaffe, B. Denker, and W. M. Yen, Phys. Rev. B 43, 5234 (1991).

[24]G. Fasol, W. Hackenberg, H. P. Hughes, K. Ploog, E. Bauser, and H. Kano, Phys. Rev. B 41, 1461 (1990).

[25]K. R. Hoffman, S. M. Jacobsen, J. Casas-Gonzalez, and W. M. Yen, in *OSA Proceedings of the Advanced Solid-State Lasers,* edited by G. Dubé and L. Chase (Optical Society of America, Washington, D.C., 1991).

[26]V. Devarajan and E. Funck, J. Chem. Phys. 62, 3406 (1975).

[27]V. Petricevic, S. K. Gayen, and R. R. Alfano, *OSA Proceedings of the Advanced Solid-State Lasers,* edited by M. L. Shand and H. P. Jenssen (Optical Society of America, Washington, D.C., 1989), Vol. 15, p. 77.